Heat transfer effects on cilia-assisted flow of viscoelastic nanofluid under an inclined magnetic field: Lubrication approximations

Khurram Javid[a], Kamel Al-Khaled[b], Saleem Khan[a], Sami Ullah Khan[c,*], Nesrine Zahi[d], Chemseddine Maatki[e], Karim Kriaa[f] , Lioua Kolsi[g,h]

[a]Department of Mathematics, Northern University, Wattar-Wallai Road, Nowshera, 24110, KPK, Pakistan

[b]Department of Mathematics & Statistics, Jordan University of Science and Technology, P.O. Box 3030, Irbid 22110, Jordan

[c,*]Department of Mathematics, Namal University, Mianwali 42250, Pakistan

[d]Applied College, Huraymila , Imam Mohammad Ibn Saud Islamic University (IMSIU), KSA,

[e]Department of Mechanical Engineering, College of Engineering, Imam Mohammad Ibn Saud Islamic University, Riyadh 11432, Saudi Arabia

[f]Department of Chemical Engineering, College of Engineering, Imam Mohammad Ibn Saud Islamic University (IMSIU) Riyadh 11432, Saudi Arabia

[g]Department of Mechanical Engineering, College of Engineering, University of Ha'il, Ha'il City, 81451, Saudi Arabia

[h]Laboratory of Metrology and Energy Systems, Energy Engineering Department, National Engineering School, University of Monastir, Monastir5000, Tunisia

***Corresponding author:** samiullah@namal.edu.pk (+923137141665)

Abstract: A numerical study has been investigated for magnetohydrodynamics (MHD) pumping of viscoelastic nanofluid by means of heat transfer in a complex ciliated channel. The Jeffrey model is followed as a non-Newtonian fluid (blood) in current investigations because of its dual characteristics: one is viscosity effects and the second is elastic in nature. The fluid motion is parallel to the direction of metachronal waves. The metachronal waves are mobilized by the cilia transport. The magnetic force reflection with horizontal angle in inclined direction is implemented. The system identifying via distinct equations is expressed in wave frame which is further normalized the flow system by using scaling quantities. In the next step, the normalized form of rheological equations will be reduced by using lubrication approximations. The ND computational tool is implemented for simulation process. The fluid transportation is controlled

by wave number, eccentric parameter of cilia, ciliated length, inclined magnetic force and non-Newtonian parameter.

Keywords: Jeffrey nanofluid; complex metachronal waves; inclined magnetic field; chemical reaction; numerical simulations.

1. Introduction

In the medical-engineering domain, the word cilia is frequently utilized in view of eukaryotic cells referring to eyelashes. They are found on the micro-organism surface and describe the same beating configuration. The shape and structure of cilia elements, particularly hair looks motile appendages, which is commonly attributed in digestive as well as reproductive systems of males and females. Cilia transportation has a vibrant act in different physiological phenomena such as reproduction, inhalation, sustenance and locomotion. The cilia elements generate the metachronal waves that are promulgates beside the channel length. The core application of these waves is to control fluid transportation and also claim dynamical impact in enriching the liquid propulsion. Additionally, they played effectively while dealing with non-viscous physiological liquids. The theory of cilia was first presented in 1675 by the Dutch. But, for two decades, comprehensive research work related to examining the cilia structure is done. In recent times, Vilfan et al. [1] detailed the effective actuation of the simulated nanometer cilia structures. Some researchers explored via analytical tool and numerical attribution regarding the ciliated transportation in numerous circumstances with different biological materials. The appliances of magnetic and heating aspect in numerous features of cilia-pumping of viscous liquid in a symmetric channel is studied by Akbar et al. [2]. They perceived that the velocity-magnitude is concentrated by increasing Lorentz force. The velocity determination is improved by increasing eccentricity of the elliptic motion. Akbar and Butt [3] investigated the Rabinowitsch fluid movement additionally endorsed with heat transmission in circular tube. The pronounced observations revealed that Newtonian fluid has the maximum magnitude at the center of tube, and it increases (decreases) with Pseudoplasticity (Dilatant) nature of the fluid. Wu et al. [4] discussed ciliated based motion in wavy propulsion channel with Carreau fluid in 2-D frame. It was being claimed that, in core regime, the pressure driven enhanced by assigning the increasing contribution of cilia-length. Cilia-assisted flow of Jeffrey liquid (blood) in a non-uniform curved path is deliberated by Javid et al. [5] under lubrication approach. It was noticed reduction in the bolus circulation under larger viscoelastic and porosity effect. They observed that viscous

impacts are foremost than the viscoelastic effects in pressure deviation subject to larger curvature effects. Maiti and Pandey [6] examined the transportation of Power-law fluid via cilia pumping following the creeping phenomenon. The peristaltic pumping is decreased for permeability constant while enhanced gradually for cilia parameter). Bhatti et al. [7] revealed attention on novel description of viscoplastic fluid in a porous planar channel via ciliated pumping. The peristaltic pumping is enhanced by increasing magnetic force. They noticed that the Newtonian liquid has a smaller pressure pumping magnitude as associated with the Casson fluid. A detailed analysis related to cilia pumping of biological fluids through numerous geometries is found in references [8–10].

Nanofluids are designed colloids involving a base liquid (e.g., air, water) and nanoparticles. Nanoparticles range in measurement somewhere in the range between 1 and 100 nm. Usually, nanofluids contain up to 5% concentration of nanoparticles to guarantee heat transfer an increment. Researchers show their interest toward the nanofluids because of their heat transfer features: they a noteworthy part in the enhancement of both thermal conductivity and connectivity over the features of base liquids. Analytical study of ciliated-assisted flow of Powell-Eyring nanoliquid in a ciliated tube under heat transfer has been studied by Agoor et al. [11]. The study is based upon lubrication theory. It was deduced that the continuation of cilia-length plays a vigorous impact in thermal assessment. Shaheen et al. [12] examined the rheology of Jeffrey nanofluid in a channel due to metachronal wave under lubrication approach. Additionally, the physical impacts of heat transfer on the flow features of cilia pumping are discussed in detail. Nadeem and Sadaf [13] theoretically performed flow analysis of nanofluid by metachronal wave in a curved channel. Exact solutions of velocity and temperature profile are obtained via integration technique under creeping phenomena. They have seen the enhancement in the pressure gradient by increasing Grashof number and radius of curvature parameter. Additionally, an asymmetric nature is noticed in the trapped bolus by the curved environment of flow geometry. Akbar et al. [14] yield out the asepcts of heat transmission subject to nanoparticles flow following the ciliated pattern in a cylindrical tube under smaller Reynolds number. Such research also highlighted the effects of porous media on the flow features of cilia pumping of nanofluid. It was observed that the Darcy’s number and slip parameter have a significant role in acceleration of axial velocity and larger in case of SWCNT in comparing to water. Hassan et al. [15] detected the thermal mechanism of nanofluid under the predication of

higher shear rate. Shafiq et al. [16] pronounced the heating improved nature of nanofluid with Riga supported configuration. Reddy et al. [17] tested the slip impact due to both velocity and thermal gradient due to nanofluid flow with porous media. The solar collected applications of nanofluid with interaction of solar systems was reported by Dhif et al. [18]. Ishtiaq et al. [19] presented the Jeffrey nanofluid flow with magnetic force impact. Bhatti et al. [20] reported the Eyring-Powell nanofluid thermal impact for optimizing the heat transfer phenomenon in asymmetric channel. The applications of nanoparticles in the drug delivery via tapered artery was focused by Bhatti et al. [21].

According to the above-mentioned literature, it is remarked that the cilia and cilia cells performed working effectively under a lubrication approach. Thus, the purpose of current research is to analyze the effects of an inclined magnetic field and chemical reactions on the nanofluid pumping in a complex ciliated channel. Akram et al. [22] discussed metachronal wave flow with Jeffrey material in 2D channel flow under implementation of lubrication theory. Nadeem and Akram [23] investigated the asymmetric surface flow governing by non-Newtonian material with inclined magnetic force via peristaltic pumping under lubrication approach. The noticed enhancement (deceleration) in velocity-magnitude by increasing angle of inclination (magnetic force). Hayat et al. [24] also used inclined magnetic force while dealing with the peristaltic pumping of Williamson fluid in an inclined channel. They utilized convective wall conditions in their rheological analysis. A similar pattern is noticed in graphs of both temperature and concentration profile by enhancing Soret and Dufour numbers. They remarked that Weissenberg number has a significant role in thermal augmentation. The combined effect of chemical reactions and a magnetic field on the biomimetic propulsion of micropolar liquid in a porous medium is studied by Barik and Dash [25]. It was noticed that the heat absorption parameter has a fruitful contribution in increasing thermal task. Shekar et al. [26] studied the physical effect of heat source and chemical reaction on the peristaltic flow of viscoelastic liquid based on role of lubrication phenomenon. The justified observations claim that the enhancement in temperature profile due to chemical reaction. Some studies regarding inclined magnetic fields are mentioned above in references [27-32], however, still some attention needed for cilia-assisted nanoparticles flow.

The transportation of Jeffrey nanofluid in a complex channel via metachronal waves is studied under lubrication approach in the current investigation. The rheological equations are derived using cartesian coordinates in the fixed frame. The motivations for using Jeffrey nonlinear model are to justify the properties of human blood. Human blood captured the shear thinning and shear thickening consequences which are successfully described by using the Jeffrey fluid model. By using linear transformation, shift the flow equation from fixed to a wave frame. The non-dimensional quantities are used to make the dimensionless system and then simplify these equations by using the lubrication approach. Due to composite form of dynamical expression, the numerical tasked is achieved via unstable and accurate NDSolve scheme via MATHEMATICA. In the last section, the graphical results for the involved parameters are presented. This presented results play interesting applications in manufacturing a nano-pumps and micro-devices based on metachronal pumping beneficial in the bio-medical industry. The results can also convey applications in the health sciences, nano-ciliated pumps, biomedical applications, radiation therapy, breaking of blood clots.

2. Mathematical modeling of blood nanofluid

A two-dimensional rheology of an incompressible viscoelastic nanoliquid in a symmetric channel is considered in the present formulation. The fluid is transported via complex sinusoidal wave trains with wave speed c present at both boundary surfaces. Let, χ be the wavelength of a metachronal wave. In the current study, rectangular coordinates $\left(\eta, \tilde{\xi}\right)$ are used. Here, η represents the channel length and $\tilde{\xi}$ transverse to the *x*-coordinate. $\gamma = \gamma_1$ and $\gamma = \gamma_2$ are considered to be upper and lower walls. The transportation is also controlled by an inclined magnetic field of strength b_0 having an angle of inclination θ with the *x*-axis. Additionally, the transport of nanofluid is controlled by thermal radiation, heat source/sink parameter and chemically reactive species. The flow diagram of symmetric ciliated channel is demonstrated in Fig. 1. The velocity components in axial and transverse directions are V and U , respectively. Mathematically, the shape of a metachronal wave (ciliated wave) can be described as [5, 8, 29, 30]:

$$H\left(\eta, \tilde{t}\right) = A + Al\left(a_1 \cos\left(b_1 \frac{\pi}{\chi}\left(\eta - c\tilde{t}\right)\right) + a_2 \cos\left(b_2 \frac{\pi}{\chi}\left(\eta - c\tilde{t}\right)\right) + a_3 \cos\left(b_3 \frac{\pi}{\chi}\left(\eta - c\tilde{t}\right)\right)\right) = \tilde{\xi}, \quad (1)$$

$$-H\left(\eta,\ \tilde{t}\right)=-A-Al\left(a_1\cos\left(b_1\frac{\pi}{\chi}\left(\eta-c\tilde{t}\right)\right)+a_2\cos\left(b_2\frac{\pi}{\chi}\left(\eta-c\tilde{t}\right)\right)+a_3\cos\left(b_3\frac{\pi}{\chi}\left(\eta-c\tilde{t}\right)\right)\right)=-\tilde{\xi}\,, \tag{2}$$

According to experimental study of Sleigh [25], that cilia tips behave in elliptical movement, and mathematically, it can be expressed as

$$\tilde{G}\left(\tilde{\eta},\eta_0,\tilde{t}\right)=\eta_0+Al\Upsilon\left(a_1\sin\left(b_1\frac{\pi}{\chi}\left(\tilde{\eta}-c\tilde{t}\right)\right)+a_2\sin\left(b_2\frac{\pi}{\chi}\left(\tilde{\eta}-c\tilde{t}\right)\right)+a_3\sin\left(b_3\frac{\pi}{\chi}\left(\tilde{\eta}-c\tilde{t}\right)\right)\right)=\tilde{\eta} \tag{3}$$

Here, A represents the mean channel width, $a_i\left(i=1-3\right)$ are amplitude ratios, $b_j\left(j=1-3\right)$ are wave parameters, $\tilde{t}$ referring to time, l be cilia length, Υ for eccentric ciliated measurement while η_0 identifying the particle position.

The mathematical expressions of the axial and transverse velocities of the cilia are [5,8]

$$\tilde{V}_0=\left.\frac{\partial\tilde{\eta}}{\partial\tilde{t}}\right|_{\eta_0}=\frac{\partial\tilde{G}}{\partial\tilde{t}}+\frac{\partial\tilde{G}}{\partial\tilde{\eta}}\frac{\partial\tilde{\eta}}{\partial\tilde{t}}=\frac{\partial\tilde{G}}{\partial\tilde{t}}+\tilde{V}_0\frac{\partial\tilde{G}}{\partial\tilde{\eta}}, \tag{4}$$

$$\tilde{U}_0=\left.\frac{\partial\tilde{H}}{\partial\tilde{t}}\right|_{\eta_0}=\frac{\partial\tilde{\xi}}{\partial\tilde{t}}+\frac{\partial\tilde{\xi}}{\partial\tilde{\eta}}\frac{\partial\tilde{\eta}}{\partial\tilde{t}}=\frac{\partial\tilde{\xi}}{\partial\tilde{t}}+\tilde{V}_0\frac{\partial\tilde{\xi}}{\partial\tilde{\eta}}, \tag{5}$$

After simplifications, alternative expressions of the above two equations (Eq. (4) and (5)) by using Eqs. (1) and (3) are given below [18]:

$$\bar{V}_0=-\frac{Al\Upsilon\frac{\pi}{\chi}c\left(a_1b_1\cos\left(b_1\frac{\pi}{\chi}\left(\tilde{\eta}-c\tilde{t}\right)\right)+a_2b_2\cos\left(b_2\frac{\pi}{\chi}\left(\tilde{\eta}-c\tilde{t}\right)\right)+a_3b_3\cos\left(b_3\frac{\pi}{\chi}\left(\tilde{\eta}-c\tilde{t}\right)\right)\right)}{1-Al\Upsilon\frac{\pi}{\chi}\left(a_1b_1\cos\left(b_1\frac{\pi}{\chi}\left(\tilde{\eta}-c\tilde{t}\right)\right)+a_2b_2\cos\left(b_2\frac{\pi}{\chi}\left(\tilde{\eta}-c\tilde{t}\right)\right)+a_3b_3\cos\left(b_3\frac{\pi}{\chi}\left(\tilde{\eta}-c\tilde{t}\right)\right)\right)},$$

$$\bar{U}_0=\frac{Al\Upsilon\frac{\pi}{\chi}c\left(a_1b_1\sin\left(b_1\frac{\pi}{\chi}\left(\tilde{\eta}-c\tilde{t}\right)\right)+a_2b_2\sin\left(b_2\frac{\pi}{\chi}\left(\tilde{\eta}-c\tilde{t}\right)\right)+a_3b_3\sin\left(b_3\frac{\pi}{\chi}\left(\tilde{\eta}-c\tilde{t}\right)\right)\right)}{1-Al\Upsilon\frac{\pi}{\chi}\left(a_1b_1\cos\left(b_1\frac{\pi}{\chi}\left(\tilde{\eta}-c\tilde{t}\right)\right)+a_2b_2\cos\left(b_2\frac{\pi}{\chi}\left(\tilde{\eta}-c\tilde{t}\right)\right)+a_3b_3\cos\left(b_3\frac{\pi}{\chi}\left(\tilde{\eta}-c\tilde{t}\right)\right)\right)}. \tag{6}$$

The Navier-Stokes equations in terms of Cartesian coordinates for the two-dimensional viscoelastic nanofluid flow are [24]:

$$\frac{\partial\tilde{V}}{\partial\tilde{\eta}}+\frac{\partial\tilde{U}}{\partial\tilde{\xi}}=0, \tag{7}$$

$$\frac{\partial \tilde{V}}{\partial \tilde{t}}+\tilde{V}\frac{\partial \tilde{V}}{\partial \tilde{\eta}}+\tilde{U}\frac{\partial \tilde{V}}{\partial \tilde{\xi}}=-\frac{1}{\varphi_f}\frac{\partial \tilde{P}}{\partial \tilde{\eta}}+\frac{1}{\varphi_f}\left(\frac{\partial \tilde{\tau}_{\tilde{\eta}\tilde{\eta}}}{\partial \tilde{\eta}}+\frac{\partial \tilde{\tau}_{\tilde{\eta}\tilde{\xi}}}{\partial \tilde{\xi}}\right)-\frac{\sigma' B_0}{\varphi_f}Cos\theta\left(\tilde{V}Cos\theta-\tilde{U}Sin\theta\right)+$$

$$\left(1-\Theta_0\right)g\Gamma\left(\tilde{\phi}-\phi_0\right)+\left(\frac{\varphi_p-\varphi_f}{\varphi_f}\right)g\Gamma'\left(\tilde{\Theta}-\Theta_0\right), \tag{8}$$

$$\frac{\partial \tilde{U}}{\partial \tilde{t}}+\tilde{V}\frac{\partial \tilde{U}}{\partial \tilde{\eta}}+\tilde{U}\frac{\partial \tilde{U}}{\partial \tilde{\xi}}=-\frac{1}{\varphi_f}\frac{\partial \tilde{P}}{\partial \tilde{\xi}}+\frac{1}{\varphi_f}\left(\frac{\partial \tilde{\tau}_{\tilde{\eta}\tilde{\xi}}}{\partial \tilde{\eta}}+\frac{\partial \tilde{\tau}_{\tilde{\xi}\tilde{\xi}}}{\partial \tilde{\xi}}\right)+\frac{\sigma' B_0}{\varphi_f}Sin\theta\left(\tilde{V}Cos\theta-\tilde{U}Sin\theta\right), \tag{9}$$

$$\frac{\partial \tilde{\phi}}{\partial \tilde{t}}+\tilde{V}\frac{\partial \tilde{\phi}}{\partial \tilde{\eta}}+\tilde{U}\frac{\partial \tilde{\phi}}{\partial \tilde{\xi}}=\gamma\left(\frac{\partial^2 \tilde{\phi}}{\partial \tilde{\eta}^2}+\frac{\partial^2 \tilde{\phi}}{\partial \tilde{\xi}^2}\right)+\frac{1}{\varphi_f \varrho_f}\left(\tilde{\tau}_{\tilde{\eta}\tilde{\eta}}\frac{\partial \tilde{V}}{\partial \tilde{\eta}}+\tilde{\tau}_{\tilde{\eta}\tilde{\xi}}\left(\frac{\partial \tilde{V}}{\partial \tilde{\xi}}+\frac{\partial \tilde{U}}{\partial \tilde{\eta}}\right)+\tilde{\tau}_{\tilde{\xi}\tilde{\xi}}\frac{\partial \tilde{U}}{\partial \tilde{\xi}}\right)-\frac{1}{\varphi_f \varrho_f}\frac{\partial q_r}{\partial \tilde{\xi}}+$$

$$\vartheta\left(D_b\left(\frac{\partial \tilde{\Theta}}{\partial \tilde{\eta}}\frac{\partial \tilde{\phi}}{\partial \tilde{\eta}}+\frac{\partial \tilde{\Theta}}{\partial \tilde{\xi}}\frac{\partial \tilde{\phi}}{\partial \tilde{\xi}}\right)+\frac{D_t}{T_0}\left(\left(\frac{\partial \tilde{\phi}}{\partial \tilde{\eta}}\right)^2+\left(\frac{\partial \tilde{\phi}}{\partial \tilde{\xi}}\right)^2\right)\right)+q_0, \tag{10}$$

$$\frac{\partial \tilde{\Theta}}{\partial \tilde{t}}+\tilde{V}\frac{\partial \tilde{\Theta}}{\partial \tilde{\eta}}+\tilde{U}\frac{\partial \tilde{\Theta}}{\partial \tilde{\xi}}=D_b\left(\frac{\partial^2 \tilde{\Theta}}{\partial \tilde{\eta}^2}+\frac{\partial^2 \tilde{\Theta}}{\partial \tilde{\xi}^2}\right)+\frac{D_t}{T_m}\left(\frac{\partial^2 \tilde{\phi}}{\partial \tilde{\eta}^2}+\frac{\partial^2 \tilde{\phi}}{\partial \tilde{\xi}^2}\right)-\kappa\left(\tilde{\Theta}-\Theta_0\right). \tag{11}$$

Here, $\mu,\tilde{\eta},\tilde{\xi},\mu,\tilde{V},\tilde{U},\varphi_p,\varphi_f,\tilde{\phi},\tilde{\Theta},\tilde{P},\tilde{\tau},\phi_0,\Theta_0,\varrho,D_b,D_t,\vartheta=\left(\varphi\varrho\right)_p/\left(\varphi\varrho\right)_f,g,\Gamma,\Gamma',\varrho_p,B_0,\sigma',\theta,\kappa$ and q_0 represent dynamic viscosity, axial component, transverse component, viscosity, axial velocity, transverse velocity, particle density, fluid density, temperature profile, nanoparticle phenomena, pressure, Cauchy stress tensor, ambient values of the temperature profile, ambient values of mass concentration, volumetric expansion coefficient, Brownian coefficient, thermophoretic diffusion, ratio of capability of effective heating nanoparticles to base fluid, thermal coefficient, concentration factor, volumetric expansion coefficient, magnetic intensity, electric conductivity, angle of inclined magnetic field with $\eta-$axis, reactive species factor and additional heat source, respectively.

For the viscoelastic fluid, defining extra stress tensor [26, 27]:

$$\tilde{\tau}=\frac{\mu}{1+\alpha}\left(\dot{\Upsilon}+\alpha'\ddot{\Upsilon}\right). \tag{12}$$

Here, α be relaxation to retardation times ratio, α' identifying the retardation time, $\dot{\Upsilon}$ expressing shear rate (dot indicate differentiation w.r.t time) and $\ddot{\Upsilon}$ is a material derivative of shear rate. The key purpose to choose this model is because of its dual features: one is viscous and the second is elasticity, which the Newtonian model cannot depict.

The definition of extra stress tensor is [29]:

$$\tau_{\eta\eta}=\frac{2\mu}{1+\alpha}\left(1+\alpha'\left(\frac{\partial}{\partial\tilde{t}}+\tilde{V}\frac{\partial}{\partial\tilde{\eta}}+\tilde{U}\frac{\partial}{\partial\tilde{\xi}}\right)\right)\frac{\partial\tilde{V}}{\partial\tilde{\eta}}, \tag{13-a}$$

$$\tau_{\eta\xi}=\frac{\mu}{1+\alpha}\left(1+\alpha'\left(\frac{\partial}{\partial\tilde{t}}+\tilde{V}\frac{\partial}{\partial\tilde{\eta}}+\tilde{U}\frac{\partial}{\partial\tilde{\xi}}\right)\right)\left(\frac{\partial\tilde{V}}{\partial\tilde{\xi}}+\frac{\partial\tilde{U}}{\partial\tilde{\eta}}\right), \tag{13-b}$$

$$\tau_{\xi\xi}=\frac{2\mu}{1+\alpha}\left(1+\alpha'\left(\frac{\partial}{\partial\tilde{t}}+\tilde{V}\frac{\partial}{\partial\tilde{\eta}}+\tilde{U}\frac{\partial}{\partial\tilde{\xi}}\right)\right)\frac{\partial\tilde{U}}{\partial\tilde{\xi}}. \tag{13-c}$$

For small temperature difference between fluid particles, defining the radiative heat flux as follows:

$$q_r=-\frac{4\varsigma}{3\mathrm{K}}\frac{\partial\tilde{\phi}^4}{\partial\tilde{\xi}}, \tag{14}$$

with K (mean absorption) and ς (Stefan-Boltzmann factor).

Furthermore, the mathematical relation between two frames: one is the wave frame and the second is a fixed frame is defined as [30]:

$$\tilde{\eta}'=\tilde{\eta}-c\tilde{t},\tilde{\xi}'=\tilde{\xi},P'(\tilde{\eta}')=\tilde{P}(\tilde{\eta},\tilde{t}),\tilde{v}'=\tilde{V}-c,\tilde{u}'=\tilde{U},\tilde{\phi}'=\tilde{\phi},\tilde{\Theta}'=\tilde{\Theta}. \tag{15}$$

Introducing the non-dimensional variables to scaling the flow features:

$$\eta=\frac{\tilde{\eta}'}{\chi},y=\frac{\tilde{\xi}'}{A},v=\frac{\tilde{v}'}{\mathrm{c}},u=\frac{\tilde{u}'}{\delta\mathrm{c}},t=\frac{\Omega\tilde{t}}{\chi},P=A^2\frac{\tilde{P}'}{c\chi\mu},\phi=\frac{\phi'-\phi_0}{\phi_1-\phi_0},\Theta=\frac{\Theta'-\Theta_0}{\Theta_1-\Theta_0},Gr=\frac{(1-\Theta_0)\varphi_f g\Gamma A^2(\phi'-\phi_0)}{\mathrm{c}\mu},$$

$$Gm=\frac{(\varphi_p-\varphi_f)g\Gamma' A^2(\phi_1-\phi_0)}{\mathrm{c}\mu_{nf}},nb=\frac{\zeta d_b(\Theta_1-\Theta_0)}{\vartheta},nt=\frac{\vartheta D_t(\phi_1-\phi_0)}{\Theta_0\upsilon},a_i=\frac{a_i}{A}(i=1-3),R_e=\frac{cA}{\upsilon},\delta=\frac{A}{\chi},$$

$$h=\frac{\tilde{H}}{A},-h=-\frac{\tilde{H}}{A},rn=\frac{16\varsigma\phi_0}{3\mathrm{K}\mu\varrho_f},pr=\frac{\mu\varrho_f}{\gamma},\sigma=\frac{q_0A^2}{\gamma(\phi_1-\phi_0)},Ec=\frac{c^2}{(\phi_1-\phi_0)\varrho_f},\xi=\frac{\kappa A^2}{D_b},Ha=B_0A\sqrt{\frac{\sigma'}{\varphi_f}},$$

$$br=EcPr,\tau_{ij}=\frac{A}{\mathrm{c}\mu}\tilde{\tau}_{\tilde{i}\tilde{j}}. \tag{16}$$

Here, $\eta,y,v,u,t,P,\phi,\Theta,Gr,Gm,nb,nt,a_i,R_e,\delta,h,-h,rn,Pr,\sigma,Ec,\xi,Ha,br$ & τ_{ij} represent axial component, transverse coordinate, axial velocity, transverse velocity, time, pressure, temperature profile, nanoparticle phenomena, Grashof number, nanofluid Grashof constant, Brownian parameter, thermophoretic coefficient, distinct amplitudes, Reynolds constant, wave constant, upper surface, lower regime, Prandtl number, heat source parameter, Eckert factor, reaction

constant, Hartmann number, Brinkman coefficient, and extra-stress tensor components, respectively.

Defining the stream functions as $v=\psi_y, u=-\delta\psi_\eta$ then Eqs. (13-16) are simplified as [30]:

$$-\frac{\partial P}{\partial \eta}+\frac{\partial \tau_{\eta y}}{\partial y}+Gr\phi+Gm\Theta-Ha^2Cos^2\theta\left(v+1\right)=0, \tag{17}$$

$$-\frac{\partial P}{\partial y}=0, \tag{18}$$

$$\left(1+rnpr\right)\frac{\partial^2\phi}{\partial y^2}+br\tau_{\eta y}\frac{\partial v}{\partial y}+nbpr\frac{\partial\Theta}{\partial y}\frac{\partial\phi}{\partial y}+ntpr\left(\frac{\partial\phi}{\partial y}\right)^2+\sigma=0, \tag{19}$$

$$\frac{\partial^2\Theta}{\partial y^2}+\frac{nt}{nb}\frac{\partial^2\phi}{\partial y^2}-\xi\Theta=0. \tag{20}$$

Where, $\tau_{\eta y}=\left(\frac{1}{1+\alpha}\right)\frac{\partial v}{\partial y}$ and $v=\frac{\partial\psi}{\partial y}$.

Apply a cross derivative between (17) & (18) in order to remove the pressure term from Eq. (17). Then, we get a simplified form of Eq. (17) and (19) as:

$$\left(\frac{1}{1+\alpha}\right)\frac{\partial^4\psi}{\partial y^4}+Gr\frac{\partial\phi}{\partial y}+Gm\frac{\partial\Theta}{\partial y}-Ha^2Cos^2\theta\frac{\partial^2\psi}{\partial y^2}=0, \tag{21}$$

$$\left(1+RnPr\right)\frac{\partial^2\phi}{\partial y^2}+Br\left(\frac{1}{1+\alpha}\right)\left(\frac{\partial^2\psi}{\partial y^2}\right)^2+NbPr\frac{\partial\Theta}{\partial y}\frac{\partial\phi}{\partial y}+NtPr\left(\frac{\partial\phi}{\partial y}\right)^2+\sigma=0. \tag{22}$$

The associate boundary conditions are [30]:

$$\psi=\frac{q}{2},\frac{\partial\psi}{\partial y}=\frac{-1}{1-\pi Al\Upsilon\left(a_1b_1\cos\left(b_1\eta\right)+a_2b_2\cos\left(b_2\eta\right)+a_3b_3\cos\left(b_3\eta\right)\right)},\ \phi=0,\ \Theta=0,\ \text{at}\ y=h, \tag{23-a}$$

$$\psi=-\frac{q}{2},\frac{\partial\psi}{\partial y}=\frac{-1}{1-\pi Al\Upsilon\left(a_1b_1\cos\left(b_1\eta\right)+a_2b_2\cos\left(b_2\eta\right)+a_3b_3\cos\left(b_3\eta\right)\right)},\ \phi=1,\ \Theta=1,\ \text{at}\ y=-h. \tag{23-b}$$

3. Results and Discussions

The two-dimensional steady magneto-hydrodynamic flow of viscoelastic nanofluid with heat transfer and chemical reaction has been examined numerically. This section defining justification to comprehensively discuss the physical effects of embedded parameters such as chemical

reaction (ξ), ratio of time relaxation and retardation (α), Hartmann number (Ha), Brownian motion (nb), Thermophoresis (nt), radiation parameter (rn), Prandtl number (pr), Brinkman number (br), Heat Source/Sink parameter (σ), cilia-length parameter (l), volumetric flow rate (q) and inclination angle (θ) on the flow features. The flow analysis is carried out with constant numerical values like $A=0.6, Gr=0.5, Gm=0.5, \alpha=0.1, nt=0.5, Ha=5, rn=1, nb=5, pr=1, \xi=0.1,$ $\eta=\pi/3, q=1, \sigma=0.1, a_1=0.3, a_2=0.4, a_3=0.5, b_1=1, b_2=2, b_3=4, l=0.1, \Upsilon=0.1, br=2$.

Figures 2(*a* – *g*) demonstrate the evolution of axial velocity $(v(y))$ with transverse coordinate (y) for variation in chemical reaction (ξ), ratio of time relaxation and retardation (α), Hartmann number (Ha), Brinkman number (br), cilia-length parameter (l), and volumetric flow rate (q). Figure 2(*a*) shows that the decreasing behavior of $v(y)$ of viscoelastic nanofluid by increasing chemical reaction (ξ) under an inclined magnetic field and radiation effects at $q=1$. The analysis observing by omitting chemical species, maximum growth of $v(y)$ is deduced as compared with the presence of chemical reaction. Physically, the presence of chemical reaction overcomes the viscoelastic effects, that why decreasing behavior is noticed in $v(y)$. The role initiated for realizing change in $v(y)$ for α is predicted via in Fig. 2(*b*). This figure is drawn under an inclined magnetic field and chemical reaction. For viscous liquid, the analysis is predicted when $\alpha=0$. Upon enriching α, the larger attention in $v(y)$ is evaluated in center regime. Moreover, enhancing significance in change of $v(y)$ is observed for viscoelastic liquid. Additionally, viscoelastic effects overcome the chemical reaction effects. Figure 2(*c*) reveals that $v(y)$ is strongly decelerated in the center by increasing magnetic force. This figure is plotted under physical effects of chemical reaction. Significantly, the magnetic force domain over the viscoelastic effects. Figure 2(*d*) presents the influences of Brinkman number (br) on $v(y)$ at $q=1$. This figure shows that increasing Brinkman number (br) from 0 to 20, a strong enhancement in $v(y)$ is observed. Moreover, the curve of $v(y)$ is shifted toward the right-side at $y=0$ by increasing Brinkman number (br). The impact of cilia-length (l) on $v(y)$ is

explored with plot of Fig. 2(*e*) under an inclined magnetic field and chemical reaction at $q=1$. This graph clearly reveals that $v(y)$ is sharply predicted upon rescaling cilia-length in range of 0.1 to 0.8. Such outcomes are pronounced due to dominance of cilia length over magnetic impact. Figure 2(*f*) depicts $v(y)$ distribution across the transverse length with different values of volumetric flow rate (q). This graph is plotted at four distinct values of q, say $q=-4,-2.5,2$ and 4. Upon fluctuating q from -4 to -2.5, lower profile of $v(y)$ is exhibited. It shows increasing behavior as q is increased from 2 to 4 in lower channel area. This figure illustrates that we can set the magnitude of $v(y)$ according to our wish by suitable setting the change in q. The dynamical visualization in inclination angle (θ) on axial velocity continued in Fig. 2(*g*) with chemical reaction. Here, $v(y)$ is strongly affected by increasing θ. For $\theta = Pi/2$, the magnitude of $v(y)$ is maximum and goes to decelerate by decreasing θ from $Pi/2$ to 0.

Figures 3(*a* – *g*) demonstrate the evolution of stream function $(\psi(y))$ with transverse coordinate (y) for variation in chemical reaction (ξ), ratio of time relaxation and retardation (α), Hartmann number (Ha), Brinkman number (br), cilia-length parameter (l), and volumetric flow rate (q). Figure 3(*a*) discussing an decreasing behavior of $\psi(y)$ of viscoelastic nanofluid by increasing chemical reaction (ξ) under inclined magnetic field and radiation effects at $q=1$. With zero reactive species, the magnitude of $\psi(y)$ is maximum as compared with the presence of chemical reaction. Physically, the presence of chemical reaction overcomes the viscoelastic effect that why decreasing behavior is noticed in stream function. The influences of viscoelastic parameter (α) on $\psi(y)$ is plotted in Fig. 3(*b*). This figure is drawn under an inclined magnetic field and chemical reaction. The result of Newtonian fluid (NF) for $\psi(y)$ is obtained at $\alpha=0$. Here, it is noticed that as α getting fluctuation beyond 0 to 0.5, the profile $\psi(y)$ get preferable increment in center. For viscoelastic liquid, the magnitude of stream function is greater and more predictable while comparing to viscous liquid. Additionally, viscoelastic effects overcome the chemical reaction effects. Figure 3(*c*) reveals that $\psi(y)$ is strongly decelerated in the center by

increasing magnetic force. This figure is plotted under physical effects of chemical reaction. Significantly, the magnetic force domain over the viscoelastic effects. Figure 3(*d*) presents the influences of Brinkman number (br) on $\psi(y)$ at $q=1$. This figure shows that increasing Brinkman number (br) from 0 to 20, strongly enhancement in $\psi(y)$ is observed. A shift is preserved in $\psi(y)$ in right-side at $y=0$ by increasing Brinkman number (br). The impacts of cilia-length (l) on $\psi(y)$ is demonstrated in Fig. 3(*e*) under inclined magnetic field and chemical reaction at $q=1$. This graph clearly reveals that $\psi(y)$ is sharply increasing in view of cilia-length from 0.1 to 0.8. Actually, the larger strength of cilia-length overcomes the magnetic effects. Figure 3(*f*) depicts $\psi(y)$ distribution across the transverse length with different values of volumetric flow rate (q). This graph is plotted at four distinct values of q, say $q=-4,-2.5,2$ and 4. Lower predictions are covered for $\psi(y)$ against q in the upper half of the flow geometry. It shows increasing behavior as q is increased from 2 to 4 near lower boundary. This figure illustrates that we can set $\psi(y)$ magnitude according preferable value of q. The significant effects of inclination angle (θ) on $\psi(y)$ are displayed in Fig. 3(*g*) under chemical reaction. The profile of $\psi(y)$ is strongly affected by the changing numeric value of θ. For $\theta=Pi/2$, the magnitude of $\psi(y)$ is maximum and goes to decelerate by decreasing θ from $Pi/2$ to 0.

Figures 4(*a* – *l*) demonstrate the graphs of temperature profile $(\phi(y))$ with transverse coordinate (y) for variation in chemical reaction (ξ), ratio of time relaxation and retardation (α), Hartmann number (Ha), Brownian motion (nb), Thermophoresis (nt), radiation parameter (rn), Prandtl number (pr), Brinkman number (br), Heat Source/Sink parameter (σ), cilia-length parameter (l) and volumetric flow rate (q). Figure 4(*a*) shows that the increasing behavior of $\phi(y)$ of viscoelastic nanofluid by increasing chemical reaction (ξ) from 0 to 9 under inclined magnetic field and radiation effects at $q=1$. Neglecting reactive species, the magnitude of $\phi(y)$ is minimum as compared with the presence of chemical reaction. Physically,

the presence of chemical reaction overcomes the viscoelastic effect, that why increasing behavior is noticed in $\phi(y)$. The impact of viscoelastic parameter (α) on $\phi(y)$ is plotted in Fig. 4(*b*). This figure is drawn under inclined magnetic field and chemical reaction. The result of Newtonian fluid (NF) for $\phi(y)$ is obtained at $\alpha = 0$. Here, it is noticed that as α increases from 0 to 0.5, a lower assessment is preserved in the profile of $\phi(y)$. More compact behavior of $\phi(y)$ in exhibited for viscoelastic case as compared with the viscous fluid. Figure 4(*c*) reveals that $\phi(y)$ is strongly decelerated by increasing magnetic force. This figure is plotted under physical effects of chemical reaction. Expressively, the magnetic force domain over the viscoelastic effects. Figure 4(*d*) lead to exploring the change in $\phi(y)$ depending upon numerical values of Brownian motion (nb). The analysis is further supported with chemical reaction and magnetic force implementation. The heat function is depressed on the left side of center by accumulating Brownian motion (nb) from 1 to 5. Realistically, the Brownian movement show more strengthen in contrasting to viscoelastic feautres. A similar nature of behavior is seen for $\phi(y)$ with thermophoresis (nt) from 1 to 5 in Fig. 4(*e*) as observed in Fig. 4(*d*). Figures 4(*f*) and 4(*g*) indicate that $\phi(y)$ is concentrated by increasing radiation parameter (rn) from 0 to 8 and Prandtl number (pr) from 0 to 8 under chemical reaction, inclined magnetic field and Brownian motion. Figures 4(*h*) and 4(*i*) present the influences of Brinkman number (br) and heat source/sink parameter (σ) on $\phi(y)$ at $q = 1$. These two figures show that aggregating the Brinkman number (br) from 0 to 20 and heat source/sink parameter (σ) from 0 to 8, a strong enhancement in $\phi(y)$ is observed. The impact of cilia-length (l) on $\phi(y)$ has been incorporated via Fig. 4(*j*) subjecting to inclined magnetic field and chemical reaction at $q = 1$. This graph clearly reveals that the temperature magnitude is enhanced with increasing range of cilia-length (0.1-0.8). Moreover, dominant role of ciliated length overcomes the magnetic effects. Figure 4(*k*) depicts $\phi(y)$ distribution across the transverse length with different values of volumetric flow rate (q). This graph is plotted at four distinct values of q, say $q = -4, -2.5, 2$

and 4. The increasing (declining) magnitude of temperature profile is obtained at $=4(q=-2.5)$ and 4. This figure illustrates that we can set the temperature magnitude according to our wish by suitable setting the numeric value of q. The effects of inclination angle (θ) on the temperature profile are displayed in Fig. 4(*l*) under chemical reaction. Here, the $\phi(y)$ is fluctuated by enlarging θ. For $\theta = Pi/2$, the behavior of $\phi(y)$ is maximum and goes to decelerate by decreasing θ from $Pi/2$ to 0.

Figures 5(*a* – *l*) demonstrate the graphs of mass concentration $(\Theta(\mathrm{y}))$ with transverse coordinate (y) for variation in chemical reaction (ξ), ratio of time relaxation and retardation (α), Hartmann number (Ha), Brownian motion (nb), Thermophoresis (nt), radiation parameter (rn), Prandtl number (pr), Brinkman number (br), Heat Source/Sink parameter (σ), cilia-length parameter (l) and volumetric flow rate (q). Figure 5(*a*) shows that decreasing behavior of $\Theta(\mathrm{y})$ of viscoelastic nanofluid by increasing chemical reaction (ξ) from 0 to 12 under inclined magnetic field and radiation effects at $q=1$. In the absence of chemical reaction (at $\xi=0$), the magnitude of $\Theta(\mathrm{y})$ is maximum as compared with the presence of chemical reaction. Physically, the presence of chemical reaction overcomes the viscoelastic effects, that why decreasing behavior is noticed in $\Theta(\mathrm{y})$. The upshots of viscoelastic parameter (α) on $\Theta(\mathrm{y})$ is strategized in Fig. 5(*b*). This figure is drawn under inclined magnetic field and chemical reaction. The result of Newtonian fluid (NF) for $\Theta(\mathrm{y})$ is obtained at $\alpha=0$. Here, it is noticed that as α increases from 0 to 0.5, the magnitude of $\Theta(\mathrm{y})$ is reduced. Physically, it shows that the magnitude of $\Theta(\mathrm{y})$ of the viscoelastic nanofluid is smaller as compared with the viscous fluid. Figure 5(*c*) reveals that $\Theta(\mathrm{y})$ is strongly decelerated by increasing magnetic force. This figure is plotted under physical effects of chemical reaction. Figure 5(*d*) deals with the influence of Brownian motion (nb) on $\Theta(\mathrm{y})$ under an inclined magnetic field and chemical reaction. A compressive concentration profile with leading role of *nb* is deduced. The viscoelastic consequences play minor role when Brownian consequences are dominant. A contrasting

reflection in $\Theta(\mathrm{y})$ leads to growing thermophoresis (nt) from 1 to 5 in Fig. 5(*e*) as observed in Fig. 5(*d*). Figures 5(*f*) and 5(*g*) indicate that the length of $\Theta(\mathrm{y})$ is reduced by swelling radiation parameter (rn) from 0 to 8 and Prandtl number (pr) from 0 to 8 under chemical reaction, inclined magnetic field and Brownian motion. Substantially, the larger strength of radiation parameter and Prandtl number overcomes the chemical reaction. Figures 5(*h*) and 5(*i*) present the influences of Brinkman number (br) and Heat Source/Sink parameter (σ) on $\Theta(\mathrm{y})$ at $q=1$. These two figures show that aggregating Brinkman number (br) from 0 to 20 and heat source/sink parameter (σ) from 0 to 8, a strong enhancement in $\Theta(\mathrm{y})$ is observed. The dynamical profile of $\Theta(\mathrm{y})$ subject to ciliated length (l) is identifying via Fig. 5(*j*) under inclined magnetic field and chemical reaction at $q=1$. This graph clearly reveals that $\Theta(\mathrm{y})$ is enhanced by growing the ciliated length. Figure 5(*k*) depicts $\Theta(\mathrm{y})$ distribution across the transverse length with different values of volumetric flow rate (q). This graph is plotted at four distinct values of q, say $q=-4,-2.5,2$ and 4. The increasing/reducing change in $\Theta(\mathrm{y})$ is claimed for specific values of q. This figure illustrates that we can set $\Theta(\mathrm{y})$ magnitude according to our wish by suitable values of *q*. The contribution of θ on $\Theta(\mathrm{y})$ is displayed in Fig. 5(*l*) under chemical reaction. Here, the length of $\Theta(\mathrm{y})$ is strongly affected by changing θ. For $\theta=Pi/2$, the length of $\Theta(\mathrm{y})$ is minimum and goes to accelerate by decreasing θ from $Pi/2$ to 0.

4. Conclusions

The mathematical formulation investigated the impact of chemical responses and inclined magnetic field on transportation of an incompressible and viscoelastic nanofluid. The motion of nanofluid takes place via complex metachronal waves (ciliated propulsion). The numerical solutions of system is followed in view of larger wavelength and lubrication approaches. The obtained solution is graphically plotted via Mathematica software 11.0 and discussed in detail. The velocity, stream function, temperature and mass concentration profiles are discussed for variations in numerous flow parameters. The key outcomes of this study are given below:

- The enhancement in stream function as well as velocity is governed to viscoelastic parameter, cilia-length parameter and Brinkman number.
- A decreasing change in velocity and stream function have been observed for increasing chemical reaction and Hartmann number.
- The temperature of the viscoelastic nanofluid is enhanced for reaction constant, Brinkman number and cilia-length parameter.
- Lower assessment in temperature profile is observed for viscoelastic parameter and magnetic parameter.
- Mass concentration of the viscoelastic nanofluid is decreased by increasing chemical reaction, viscoelastic parameter, magnetic parameter, radiation parameter, Prandtl number and Brownian motion. A reverse trend is observed by enhancing Brinkman number, cilia-length and external heating source.
- In the absence of an inclination angle, the maximum magnitude of velocity profile, stream function, heat and mass concentration are obtained.
- A controls of blood flow is noticed for larger magnetic force.
- All graphs are plotted by using fixed values of involved parameters:

$$A=0.6, Gr=0.5, Gm=0.5, \alpha=0.1, nt=0.5, Ha=5, rn=1, nb=5, pr=1, \xi=0.1, \eta=\frac{\pi}{3}, q=1,$$
$$\sigma=0.1, a_1=0.3, a_2=0.4, a_3=0.5, b_1=1, b_2=2, b_3=4, l=0.1, \Upsilon=0.1, br=2 \ \&\theta=\pi/3.$$

FIGURES AND TABLES CAPTIONS

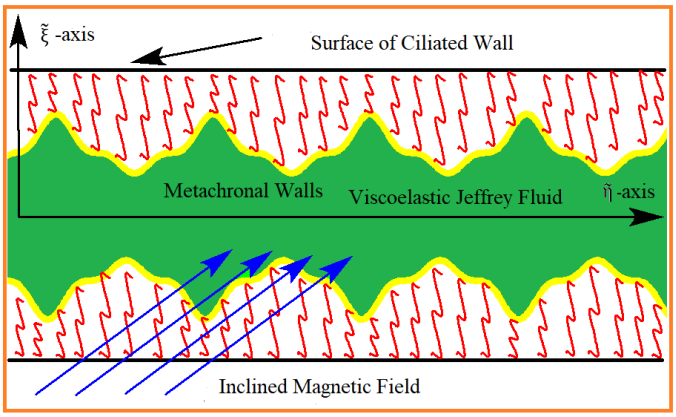

Fig. 1: Flow diagram.

(a) (b)

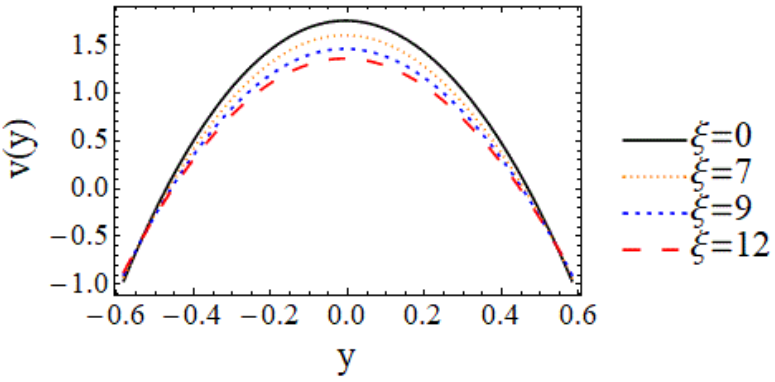

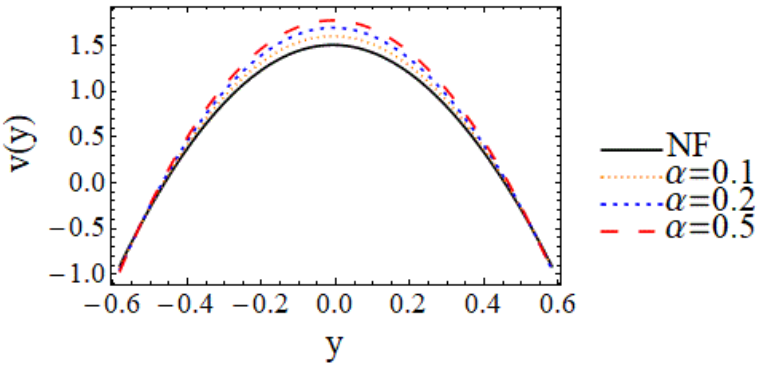

(c) (d)

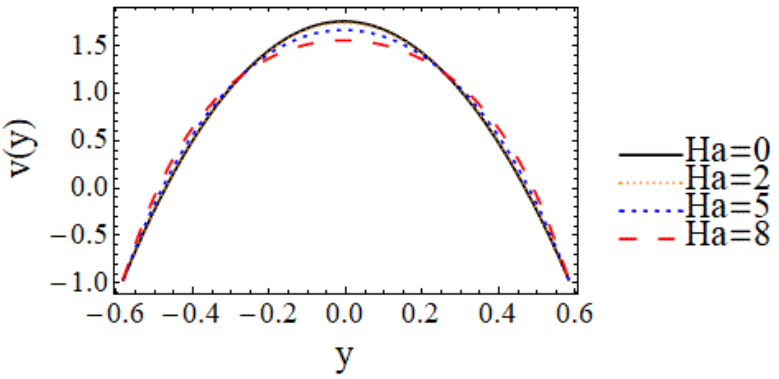

(e)

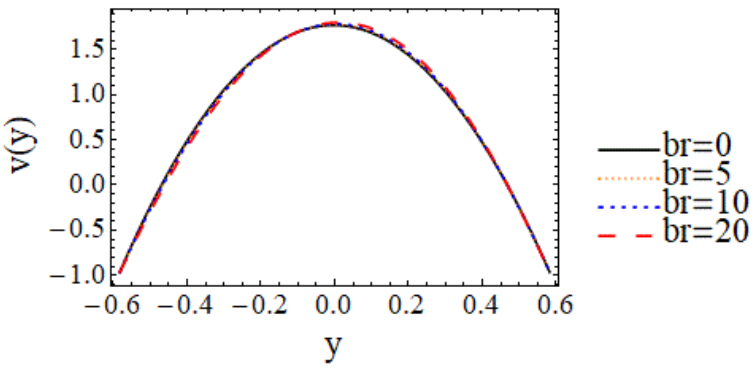

(f)

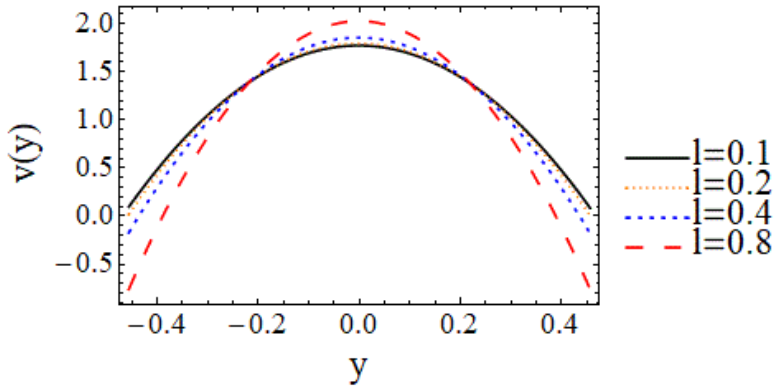

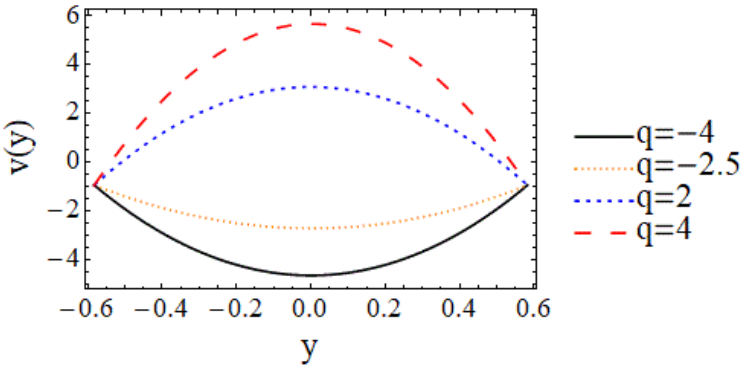

(g)

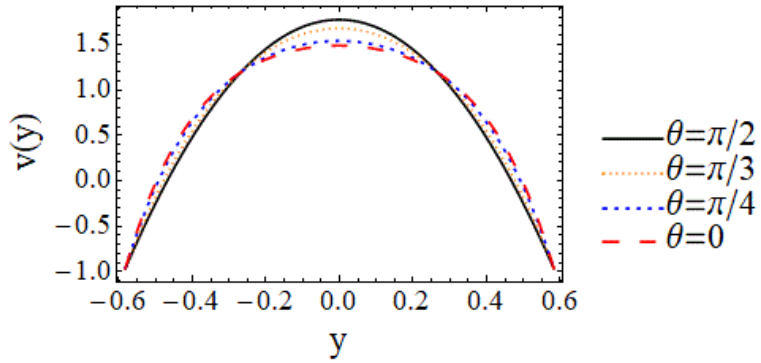

Fig. 2(a-g): (**a**) Velocity profile for chemical reaction (**ξ**), (**b**) Velocity profile for viscoelastic parameter (**α**), (**c**) Velocity profile for Hartmann number (**Ha**), (**d**) Velocity profile for

Brinkman number (**br**), (**e**) Velocity profile for cilia-length parameter (**l**), (**f**) Velocity profile for cross-section area (**q**) and (**g**) Velocity profile for inclination angle (**θ**).

(a)

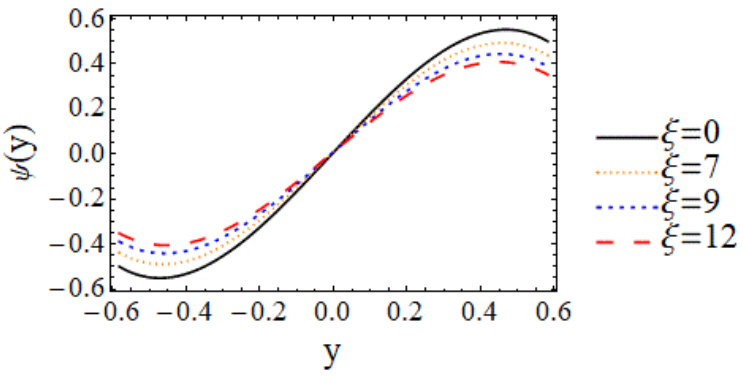

(b)

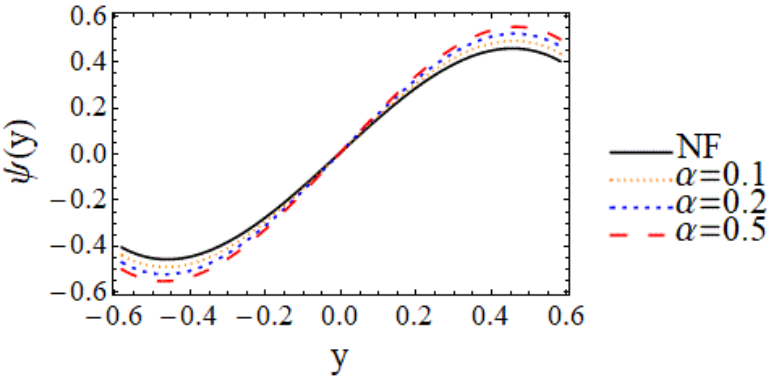

(c)

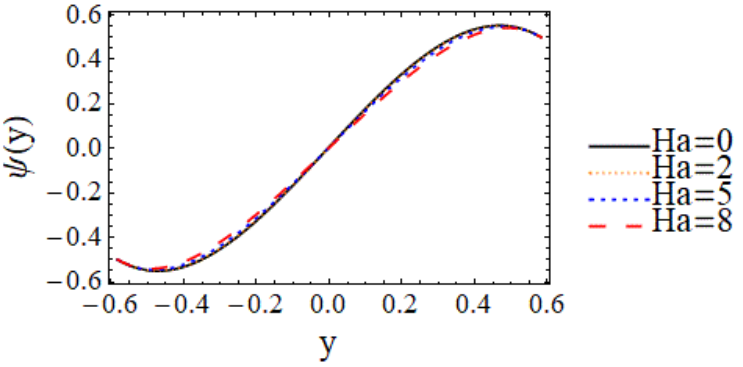

(d)

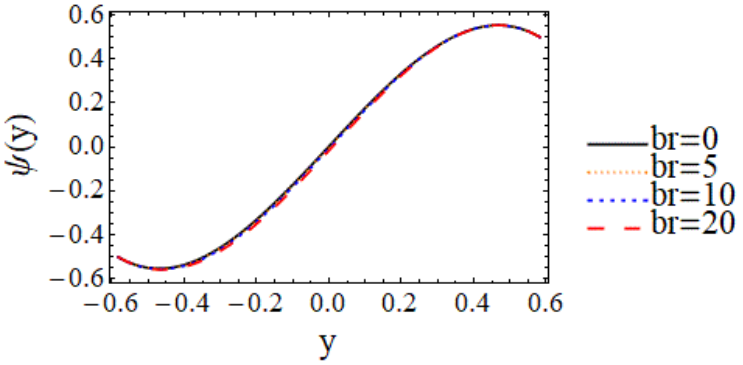

(e)

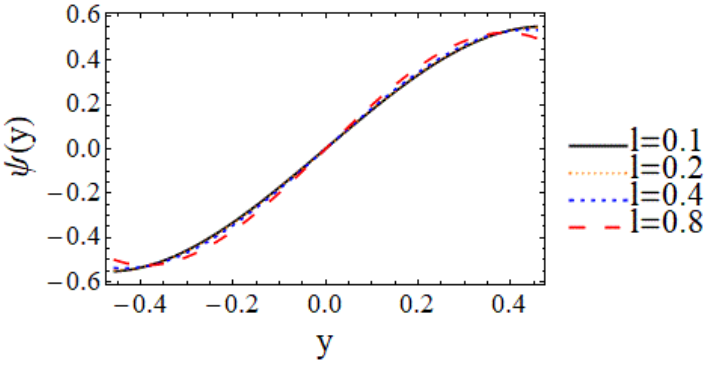

(f)

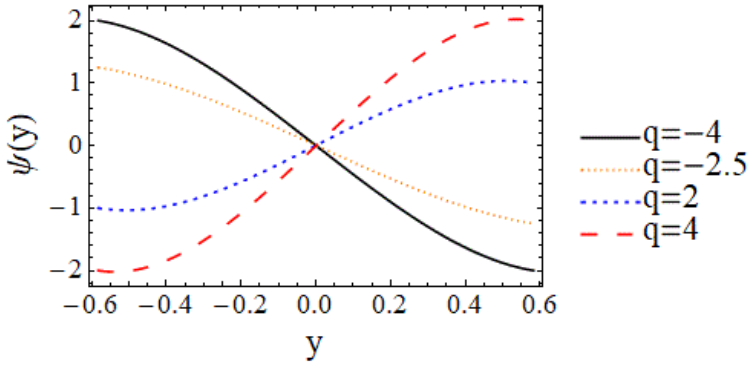

(g)

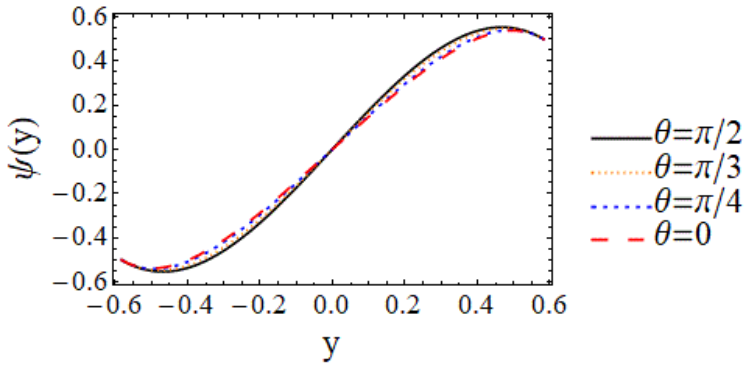

Fig. 3(a-g): (**a**) Steam function for chemical reaction (**ξ**), (**b**) Steam function for viscoelastic parameter (**α**), (**c**) Steam function for Hartmann number (**Ha**), (**d**) Steam function for Brinkman number (**br**), (**e**) Steam function for cilia-length parameter (**l**), (**f**) Steam function for cross-section area (**q**) and (**g**) Steam function for inclination angle (**θ**).

(a)

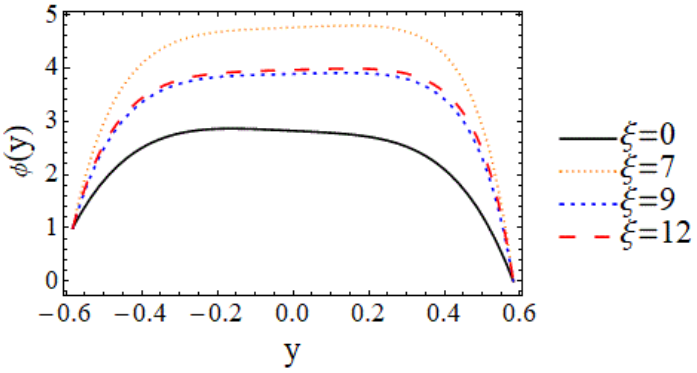

(b)

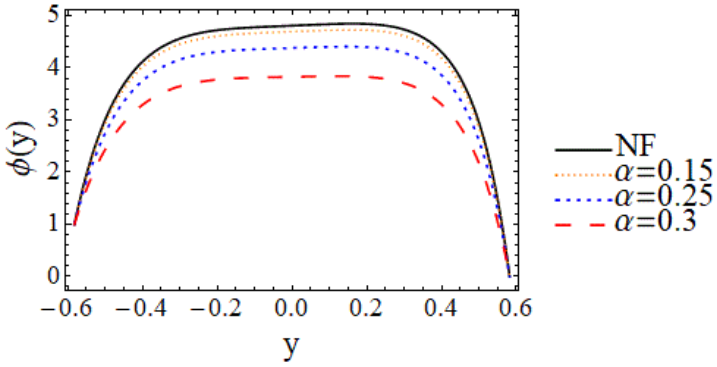

(c)

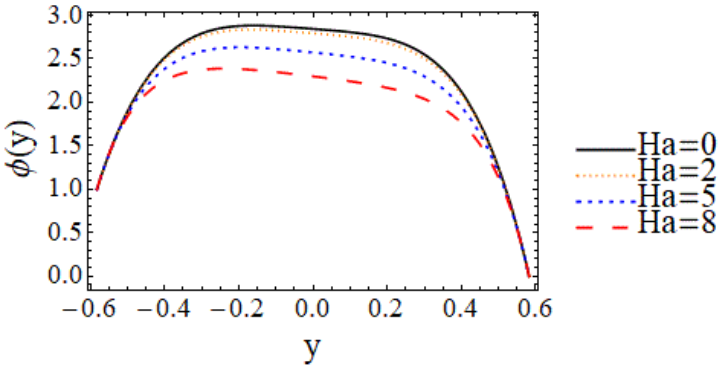

(d)

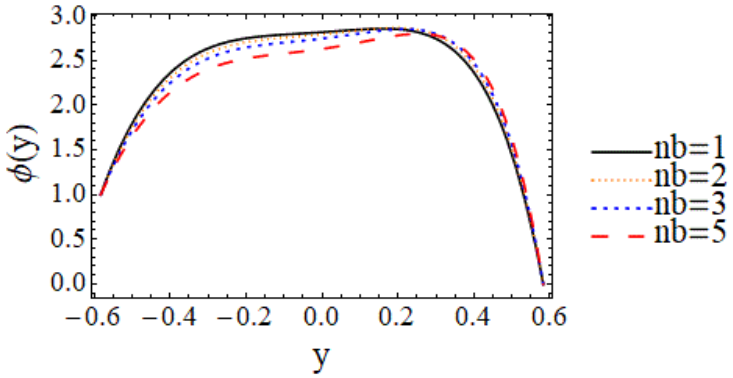

(e)

(f)

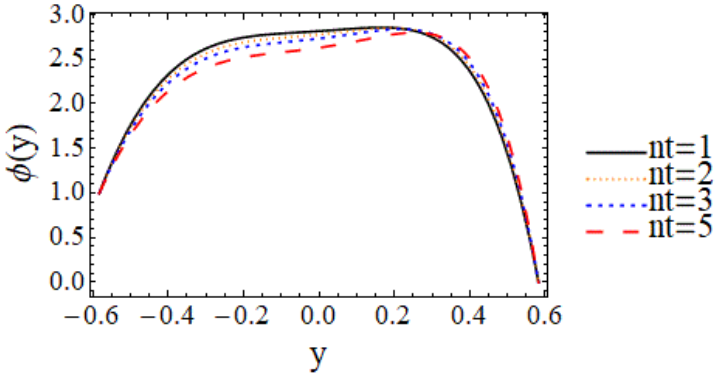
ϕ(y)
y
nt=1
nt=2
nt=3
nt=5

(g)

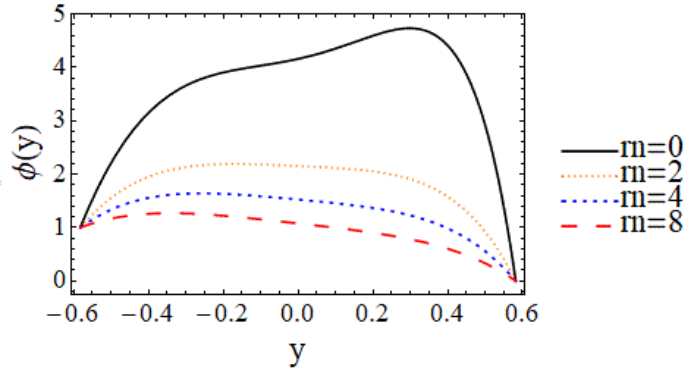
ϕ(y)
y
rn=0
rn=2
rn=4
rn=8

(h)

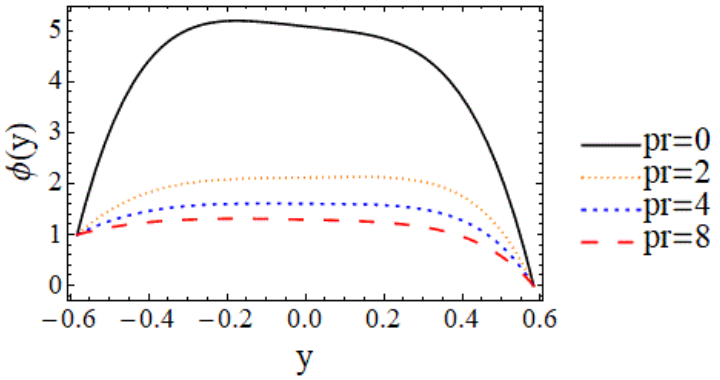
ϕ(y)
y
pr=0
pr=2
pr=4
pr=8

(i)

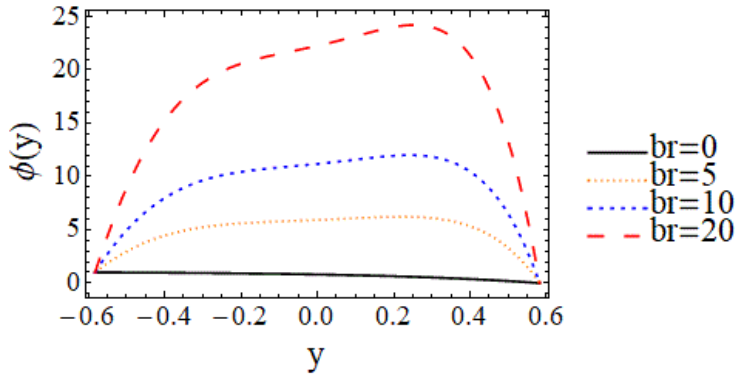
ϕ(y)
y
br=0
br=5
br=10
br=20

(j)

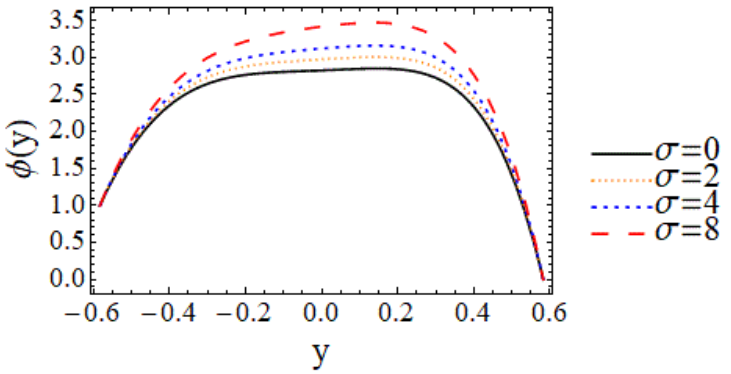
ϕ(y)
y
σ=0
σ=2
σ=4
σ=8

(k)

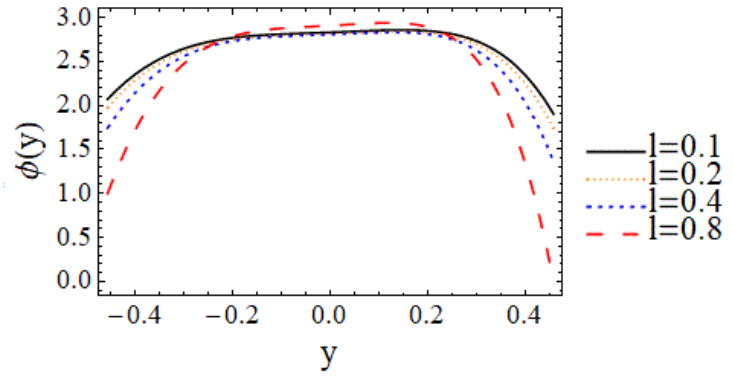
ϕ(y)
y
l=0.1
l=0.2
l=0.4
l=0.8

(l)

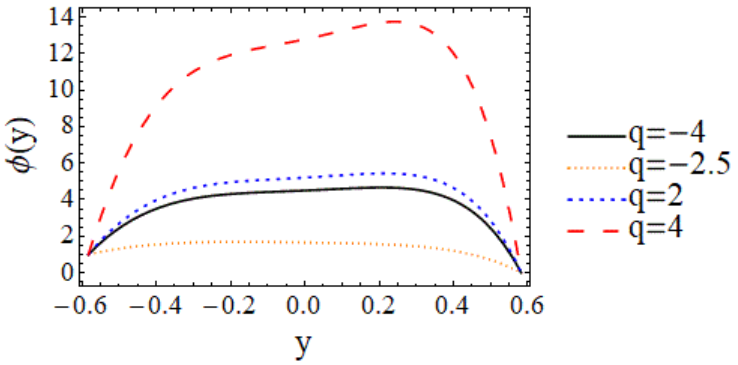
ϕ(y)
y
q=−4
q=−2.5
q=2
q=4

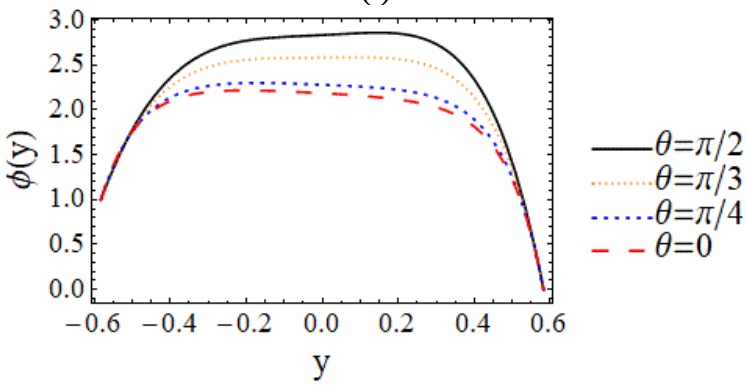
ϕ(y)
y
θ=π/2
θ=π/3
θ=π/4
θ=0

Fig. 4(a-l): (**a**) Temperature profile for chemical reaction (**ξ**), (**b**) Temperature profile for viscoelastic parameter (**α**), (**c**) Temperature profile for Hartmann number (**Ha**), (**d**) Temperature profile for Brownian motion (**nb**), (**e**) Temperature profile for Thermophoresis parameter (**nt**), (**f**) Temperature profile for radiation parameter (**rn**), (**g**) Temperature profile for Prandtl number (**pr**), (**h**) Temperature profile for Brinkman number (**br**), (**i**) Temperature profile for Heat source/Sink parameter (**σ**), (**j**) Temperature profile for cilia-length parameter (**l**), (**k**) Temperature profile for cross-section area (**q**) and (**l**) Temperature profile for inclination angle (**θ**).

(a)

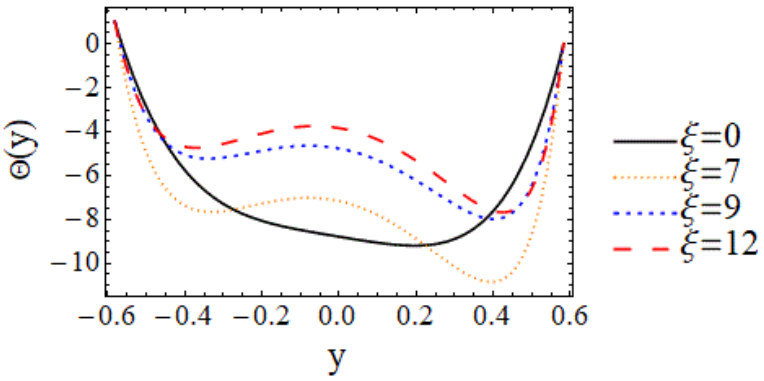

(b)

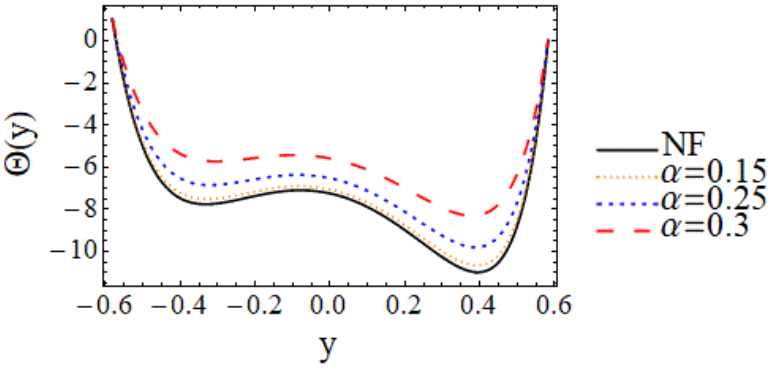

(c)

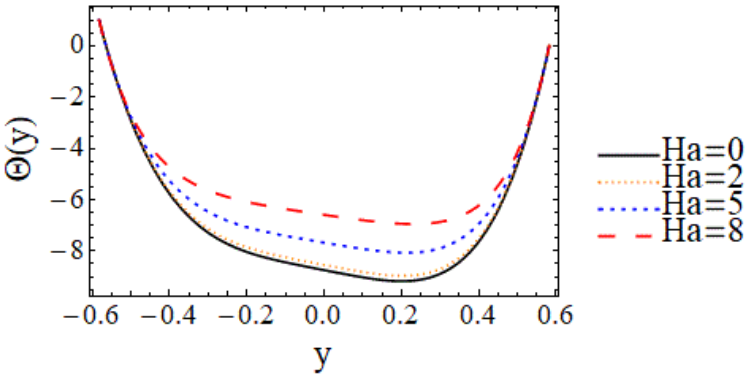

(d)

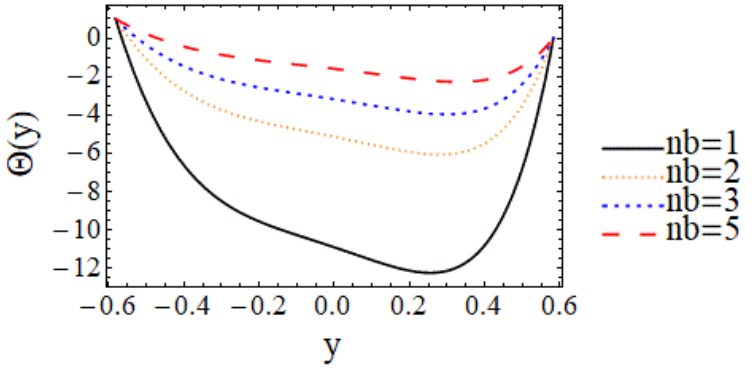

(e)

(f)

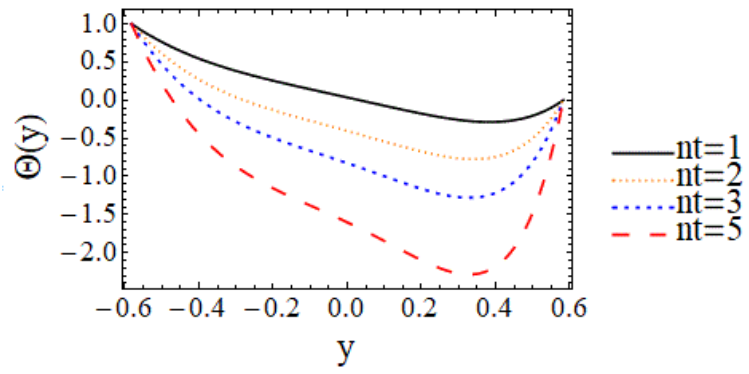
Θ(y)
y
nt=1
nt=2
nt=3
nt=5

(g)

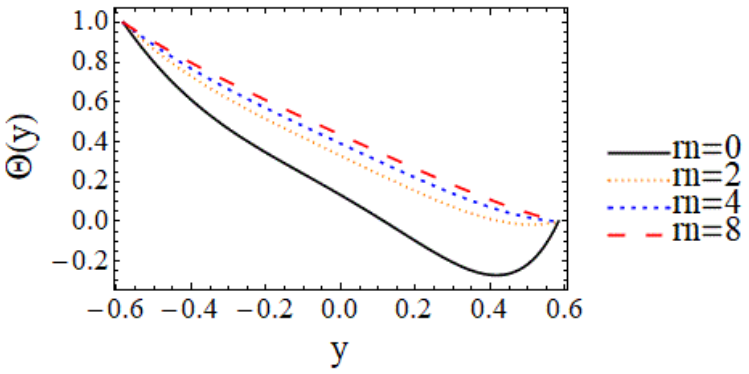
Θ(y)
y
rn=0
rn=2
rn=4
rn=8

(h)

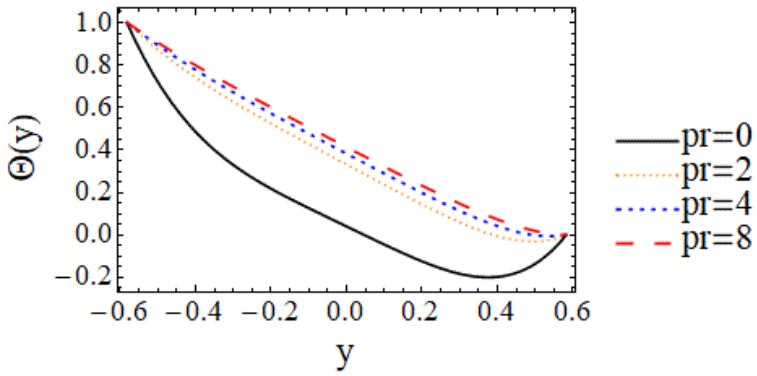
Θ(y)
y
pr=0
pr=2
pr=4
pr=8

(i)

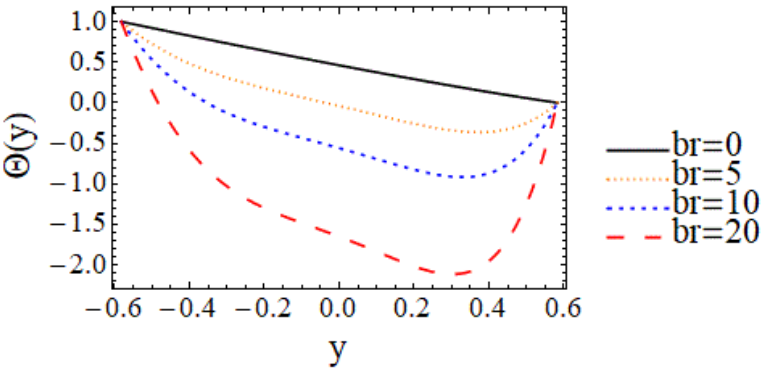
Θ(y)
y
br=0
br=5
br=10
br=20

(j)

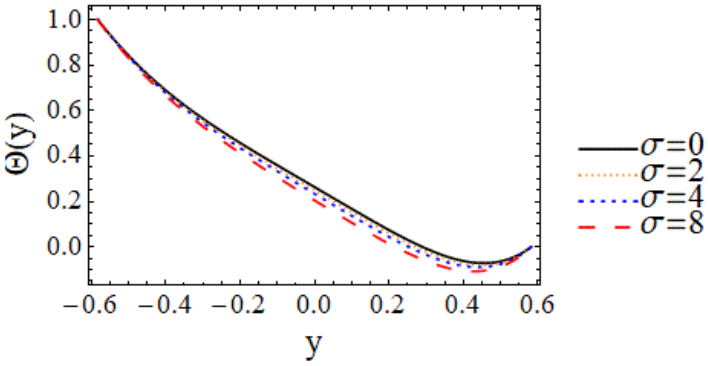
Θ(y)
y
σ=0
σ=2
σ=4
σ=8

(k)

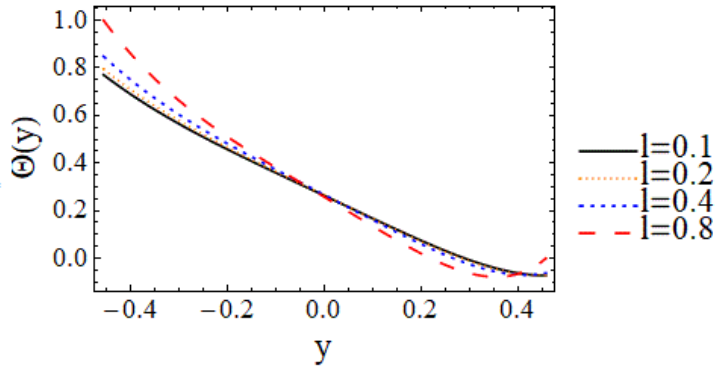
Θ(y)
y
l=0.1
l=0.2
l=0.4
l=0.8

(l)

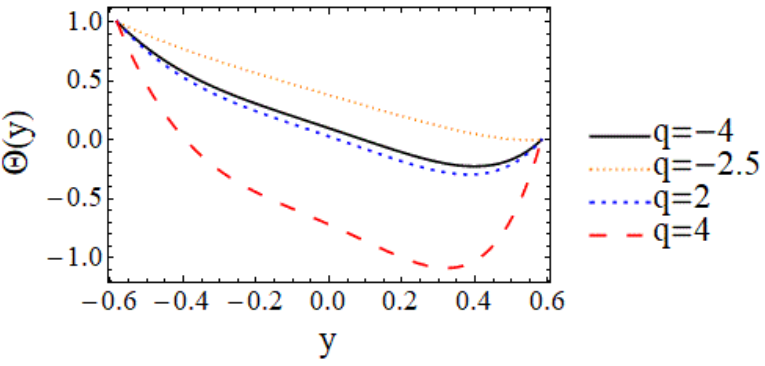
Θ(y)
y
q=−4
q=−2.5
q=2
q=4

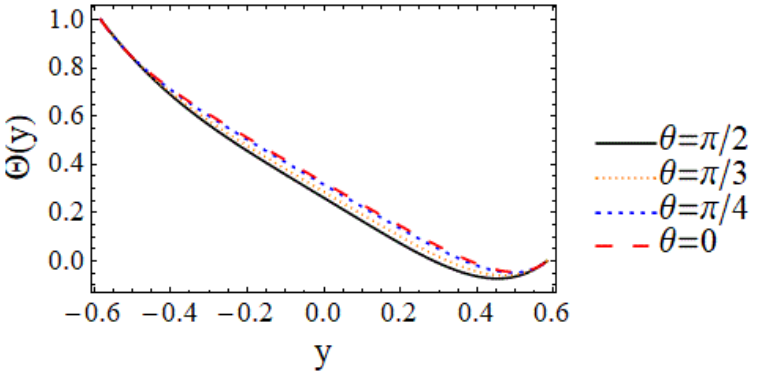
Θ(y)
y
θ=π/2
θ=π/3
θ=π/4
θ=0

Fig. 5(a-l): (**a**) Mass concentration for chemical reaction (**ξ**), (**b**) Mass concentration for viscoelastic parameter (**α**), (**c**) Mass concentration for Hartmann number (**Ha**), (**d**) Mass concentration for Brownian motion (**nb**), (**e**) Mass concentration for Thermophoresis parameter (**nt**), (**f**) Mass concentration for radiation parameter (**rn**), (**g**) Mass concentration for Prandtl number (**pr**), (**h**) Mass concentration for Brinkman number (**br**), (**i**) Mass concentration for Heat source/Sink parameter (**σ**), (**j**) Mass concentration for cilia-length parameter (**l**), (**k**) Mass concentration for cross-section area (**q**) and (**l**) Mass concentration for inclination angle (**θ**).

REFERENCES

1. Vilfan M., Kokot G., Vilfan A, et al. "Analysis of fluid flow around a beating artificial cilium", *Beilstein J Nanotechnol*. **3**, pp. 163–171 (2012).
2. Akbar, S. N., Khan, Z., Nadeem, S., "Metachronal beating of cilia under influence of Hartmann layer and heat transfer", *Eur. Phys. J. Plus*, **129**, pp. 129 (2014).
3. Akbar, N. S., Butt, A. W. "Heat transfer analysis of Rabinowitsch fluid flow due to metachronal wave of cilia", *Results Phys*., **5,** pp. 92–98 (2015).
4. Wu, A., Abbas, S., Asghar, Z. et al. "A shear-rate-dependent flow generated via magnetically controlled metachronal motion of artificial cilia", *Biomech Model Mechan.,* **19**, pp. 1713–24 (2020).
5. Javid, K., Alqsair, U. F., Hassan, M. et al. "Cilia-assisted flow of viscoelastic fluid in a divergent channel under porosity effects", *Biomech Model Mechan.,* **20**, pp. 1399–412.
6. Maiti, S., Pandey, S., "Rheological fluid motion in tube by metachronal waves of cilia", *Appl. Math. Mech.* **38**, pp. 393–410 (2017).
7. Bhatti, M., Zeeshan, A., Rashidi, M., "Influence of magnetohydrodynamics on metachronal wave of particle-fluid suspension due to cilia motion", *Eng Sci Technol Int J.* **20,** pp. 265–271 (2017).
8. Akbar, N. S., Tripathi, D. and Bég, O. A. " MHD dissipative flow and heat transfer of Casson fluids due to metachronal wave propulsion of beating cilia with thermal and velocity slip effects under an oblique magnetic field", *Acta Astronaut*, **128,** pp. 1–12 (2016).

9. Akbar NS, Khan Z, Nadeem S. Influence of magnetic field and slip on Jeffrey fluid in a ciliated symmetric channel with metachronal wave pattern. J Appl Fluid Mech 2016;9:565–7.
10. Ramesh, K., Tripathi, D., Bég, O. A. "Cilia-assisted hydromagnetic pumping of biorheological couple stress fluids," *Prop. Power Res.*, **8(3)**, pp. 221-233 (2019).
11. Agoor, B. M., Ahmed S. M. E., Alam, H. "The binary Powell-Eyring nanofluid of peristaltic flow with heat transfer in a ciliated tube", *Int. J. Fluid Mech. Therm. Sci*. **7(1)**, pp. 1-11, (2021).
12. Shaheen, S., Maqbool, K., Siddiqui, A. M. "Micro rheology of Jeffrey nanofluid through cilia beating subject to the surrounding temperature", *Rheol. Acta*, **59**, pp. 565–573 (2020).
13. Nadeem, S., Sadaf, H. "Theoretical analysis of Cu-blood nanofluid for metachronal wave of cilia motion in a curved channel", *IEEE Trans Nanobioscience*, **14**, 447–454 (2015).
14. Akbar, N.S., Shoaib, M., Tripathi, D. et al. "Analytical approach to entropy generation and heat transfer in CNT-nanofluid dynamics through a ciliated porous medium", *J. Hydrodyn*, **30**, pp. 296–306 (2018).
15. Hassan, M., Oudina, F. M., Faisal, A. et al. "Thermal energy and mass transport of shear thinning fluid under effects of low to high shear rate viscosity", *Int. J. Thermofluids*, **15,** pp. 100176, (2022).
16. Shafiq, A. Oudina, F. M., Sindhu, T. N. "Sensitivity analysis for Walters' B nanoliquid flow over a radiative Riga surface by RSM", *Scien. Iranica*, **29(3)**, pp. 1236-1249 (2022).
17. Reddy, Y. D., Oudina, F. M., Goud, B. S. et al. "Radiation, Velocity and Thermal Slips Effect Toward MHD Boundary Layer Flow Through Heat and Mass Transport of Williamson Nanofluid with Porous Medium," *Arab J Sci Eng.,* **47(12)**, pp. 16355–16369 (2022).
18. Dhif, K., Oudina, F. M., Chouf, S., et al. "Thermal Analysis of the Solar Collector Cum Storage System using a Hybrid-Nanofluids," *J. Nanofluids*, **10(4)**, pp. 634–644, (2021).
19. Ishtiaq, F., Ellahi, R., Bhatti, M.M. et al. "Insight in Thermally Radiative Cilia-Driven Flow of Electrically Conducting Non-Newtonian Jeffrey Fluid under the Influence of Induced Magnetic Field", *Mathematics*, **10(12)**, pp. 2007, (2022).

20. Bhatti, M.M., Sait, S.M.,Ellahi, R., et al. “Thermal analysis and entropy generation of magnetic Eyring-Powell nanofluid with viscous dissipation in a wavy asymmetric channel", *Int. J. Numerical Methods Heat & Fluid Flow*, **33(5)**, pp. 1609-1636.
21. Bhatti, M.M., Sait, S.M., Ellahi, R. “Magnetic Nanoparticles for Drug Delivery through Tapered Stenosed Artery with Blood Based Non-Newtonian Fluid”, *Pharmaceuticals*, **15**, pp. 1352 (2022).
22. Akram, S., Aly, E., Nadeem, S. “Effects of metachronal wave on biomagnetic Jeffery fluid with inclined magnetic field”, *Rev Téc Ing Univ Zulia*, **38**, pp. 18–28 (2015).
23. Nadeem, S., Akram, S. “Influence of inclined magnetic field on peristaltic flow of a Williamson fluid model in an inclined symmetric or asymmetric channel”, *Math. Comput Model*, **52**, pp. 107–119 (2010).
24. Chabani, Oudina, F. M., Vaidya, H. et al. “Numerical analysis of magnetic hybrid Nano-fluid natural convective flow in an adjusted porous trapezoidal enclosure”, *J. Mag. Magn. Materials*, **564 (2)**, pp. 170142, (2022).
25. Bank R, Dash G. “Chemical reaction effect on peristaltic motion of micropolar fluid through a porous medium with heat absorption in the presence of magnetic field”, *Adv Appl Sci Res.*, **6**, pp. 20–34 (2015).
26. Akram, S., Athar, M., Saeed, K., “Hybrid impact of thermal and concentration convection on peristaltic pumping of Prandtl nanofluids in non-uniform inclined channel and magnetic field”, *Case Stud Therm. Eng*. **25**, pp. 100965 (2021).
27. Akinbowale, T., Akinshilo, “Mixed convective heat transfer analysis of MHD fluid flowing through an electrically conducting and non-conducting walls of a vertical micro-channel considering radiation effect,” *Appl. Therm. Eng.*, **156**, pp. 506-513 (2019).
28. Asghar, Z., Javid, K., Waqas, M., et al. “Cilia-driven fluid flow in a curved channel: effects of complex wave and porous medium” *Fluid Dyn. Res.* **52**, pp. 015514 (2020).
29. Javid, K., Al-Khaled, K., Hassan, M. et al. “A transport of Jeffrey model viscoelastic fluid by complex peristalsis motion of nonuniform curved channel’s walls under resistance of magnetic field”, *ZAMM-J Appl Math Mech Für Angew Math Mech*, **102**, pp. e202100067 (2022).

30. Hussain, Z., Al-Khaled, K., Ashrif, U. et al. “A mathematical model for radiative peristaltic flow of Jeffrey fluid in curved channel with Joule heating and different walls: Shooting technique analysis”, *Ain Shams Eng. J.* **13**, pp. 101685 (2022).
31. Javid, K., Ellahi, M., Al-Khaled, K. et al. “EMHD creeping rheology of nanofluid through a micro-channel via ciliated propulsion under porosity and thermal effects”, *Case Stud. Therm. Eng.*, **30**, pp. 101746 (2022).
32. Imran, A., Raja, M. A. Z., Shoaib, M., “Electro-osmotic transport of a Williamson fluid within a ciliated microchannel with heat transfer analysis,” *Case Stud. Therm. Eng.*, **45**, pp. 102904, (2023).

Nomenclature

$\tilde{\eta}$	channel length
c	wave speed
$(\tilde{\eta}, \tilde{\xi})$	rectangular coordinates
$(\tilde{U}, \tilde{V})$	velocity components
A	mean channel width
a_i	amplitude ratios
b_j	wave parameters
$\tilde{t}$	time
l	cilia length
Υ	eccentric measurement of the elliptic motion of cilia
η_0	reference place of the particle.
μ	dynamic viscosity
φ_p	particle density
φ_f	fluid density
$\tilde{\phi}$	temperature profile
$\tilde{P}$	pressure
$\tilde{\tau}$	Cauchy stress tensor
ϕ_0	ambient values of the temperature profile

Θ_0 ambient values of mass concentration

ϱ volumetric expansion coefficient

D_b Brownian diffusion coefficient

D_t thermophoretic diffusion coefficient

ϑ nanoparticles effective heat capacity to fluid heat capacity ratio

q_0 heat source/sink parameter

κ chemical reaction parameter

θ angle of inclined magnetic field

σ' electric conductivity

B_0 magnetic intensity

ϱ_p volumetric expansion coefficient of nanoparticles

Γ' thermal expansion coefficient, concentration expansion coefficient

α ratio of the relaxation to retardation times

α' retardation time

$\dot{\Upsilon}$ shear rate

$\ddot{\Upsilon}$ material derivative of shear rate

τ_{ij} extra-stress tensor components

br Brinkman number

Ha Hartmann number

ξ chemical reaction

Ec Eckert number

γ heat source/sink parameter

pr Prandtl number

t time

P pressure

ϕ temperature profile

Gm Grashof number

Khurram Javid is working assistant professor in Northern University, Wattar-Wallai Road, Nowshera, Pakistan. Dr. Ahmed has published 40 research paper with impact factor 80 plus. His area of research is fluid mechanics and nanofluids. He is reviewer of 30 impact factor journals.

Kamel Al-Khaled is professor of Mathematics in the Mathematics and Statistics, Jordan University of Science and Technology, Irbid Jordan. Dr. Kamel Al-Khaled has more than 30 years teaching and research experience. His area of research is thermal energy and fractional calculus. He has published more than 150 research articles in different journal. Dr. Kamel Al-Khaled is also guest editor of some journals.

Saleem Khan is research assistant in assistant professor in Northern University, Wattar-Wallai Road, Nowshera, Pakistan. Saleem Khan research area is nanofluids and partial differential equations. Saleem Khan is also active researcher and published 5 research papers in different journals.

Sami Ullah Khan is Associate Professor in the Namal University Mianwali Pakistan. Dr. Khan has published 380 research papers with impact factor 1000 plus. He is reviewer of more than 70 impact factor journal. Dr Khan is guest editor of 4 impact factor journals. Dr Khan has been awarded as distinguish researcher from university.

Nesrine Zahi is assistant professor in Imam Mohammad Ibn Saud Islamic University, Riyadh Saudi Arabia. His area of interest is nanotechnology. Dr. Nesrine Zahi has more than 10 years of teaching an research experiences. Dr. Nesrine Zahi has published 12 research articles in different journals.

Chemseddine Maatki is working as an associate professor in department of mechanical engineering at Imam Mohammad Ibn Saud Islamic University, Riyadh Saudi Arabia. Dr. Chemseddine Maatki has received PhD degree in mechanical engineering. His research expertise is in fluid mechanics and numerical analysis. Dr. Chemseddine Maatki has published 59 research papers. He is also reviewer of many international journals.

Karim Kriaa received his PhD degree in chemical engineering. Dr. **Karim Kriaa** is the coauthor of more than 10 publications and chapter in book. He involved in Extraction and Separation chemical projects. Currently he is assistant professor in chemical Engineering, College of Engineering, Imam Mohammad Ibn Saud Islamic University (IMSIU) Riyadh, Saudi Arabia

Lioua Kolsi is an associate Professor in the University of Hail, Saudia Arabia. Dr Kolsi is working in thermal systems and published more than 300 research papers in different journals. His area of research is nanofluids, thermal engineering and computational fluid mechanics. Dr Kolsi is guest editor of applied sciences journal.